Microstructure characterization and hardness distribution of 13Cr4Ni multipass weld metal

Mohsen Mokhtabad Amrei, Hossein Monajati, Denis Thibault, Yves Verreman, Lionel Germain, Philippe Bocher

Microstructure characterization and hardness distribution of 13Cr4Ni multipass weld metal

Mohsen Mokhtabad Amrei [a,*], Hossein Monajati [a], Denis Thibault [b], Yves Verreman [c], Lionel Germain [d,e], Philippe Bocher [a]

[a] École de Technologie Supérieure, Montréal, Canada
[b] Institut de recherche d'Hydro-Québec, Montréal, Canada
[c] École Polytechnique de Montréal, Canada
[d] Université de Lorraine, Laboratoire d'Etude des Microstructures et de Mécanique des Matériaux (LEM3), UMR 7239, Metz F-57045, France
[e] Université de Lorraine, Labex DAMAS, Metz F-57045, France

ARTICLE INFO

Keywords:
13Cr4NiMo martensitic stainless steels
Multipass weld microstructure
Heat affected zone
Reformed austenite
Tempering

ABSTRACT

Multipass welding is a common method for fabrication and repairs of large industrial steel parts. In the hydroelectric industry these parts are commonly made with 13Cr4Ni steels that present outstanding performances. In this research the microstructures and crystallographic textures of a multipass weld have been studied. The microstructure was found to be complex and heterogeneous, consisting of several regions affected by adjacent weld passes. The study showed that austenite parent grains modification happened in areas close to the subsequent weld passes. However, parallel and low angle interface laths were observed inside martensite sub-blocks over different regions. The hardness profile was explained by overlaying the simple three regions heat affected zone. In some regions a tempering heat treatment effect was observed while in some other regions a double-quenching has happened.

1. Introduction

13Cr4Ni belongs to the low carbon martensitic stainless steels. They have lots of applications in hydroelectric, power generation, offshore and petrochemical industries. Multipass welding processes are common for the fabrication and repair of this steel as the carbon content is low enough to avoid loss of toughness and compressive residual stresses built in the weld after each pass [1–3]. Generally the composition of the electrode is similar to the base metal in order to produce weld metals with similar properties [4]. 410NiMo filler metal family is the best choice among available electrodes.

13Cr4Ni steel solidifies to δ-ferrite, then starts to transforms into austenite at around 1300 °C and ends, in a thermodynamically equilibrium conditions, at around 1200 °C [1,5]. At temperatures lower than 1200 °C austenite decomposes and if a thermodynamically equilibrium is achieved; ferrite and carbides are expected to be the stable phases at room temperature. However in cooling conditions which are typical of production, the very slow rate of ferrite-carbides formation maintains the austenite existence at low temperature and then austenite is subjected to the martensitic transformation.

The fully martensitic microstructure expected after cooling to room temperature, may be very complex. Alloying elements segregation in-between dendrites at the final stages of solidification can stabilize δ-ferrite phase which can remain in the microstructure even at room temperature [1]. Furthermore, the transformation of austenite to martensite can be incomplete and small amounts of retained austenite may remain between martensite laths [6–9].

The microstructure of a multipass weld is even more complex as the thermal cycles of subsequent passes act as several quick heat treatments which can affect the microstructure. As a result, some carbides and austenite can be formed or modified locally. It has been shown that the reformed austenite can be stable at room temperature and it improves toughness and fatigue properties. However, in cases of receiving excessive heat from adjacent weld passes, the reformed austenite transforms back to fresh martensite on cooling and it significantly reduces the impact properties [10–14].

The focus of this study is on the heterogeneous nature of as-welded multipass microstructures such as various heat affected regions inside weld beads and hardness distributions in order to better understand microstructure features characteristics, formations, and evolutions. Previously, and as a first step toward the goals of the current study, a

* Corresponding author at: Department of Mechanical Engineering, École de Technologie Supérieure, Montréal, QC H3C 1K3, Canada.
E-mail address: mmokhtabad@gmail.com (M.M. Amrei).

Table 1
Welding parameters.

Method	Interpass temp. (°C)	Pre-heat temp. (°C)	Voltage (V)	Current (A)	Torch speed (mm/s)	Filler deposit rate (kg/h)	Heat input (J/mm)	Welding position	Gas
Flux-core arc welded (FCAW)	200	180	21.1	209	4.5	3.9	980	1G	Argon-25% CO_2

Table 2
Nominal and measured composition of substrate metal and welding electrode (wt.%).

Grade	Cr	Ni	Mo	Si	Mn	C	P	S	Cu	N
CA6NM (ASTM)	11.5–14	3.5–4.5	0.4–1.0	<0.1	<0.5	<0.06	<0.04	<0.03	<0.05	–
CA6NM (As measured)	12.5	4.17	0.467	0.43	0.7	0.04	0.027	0.005	0.02	–
E410NiMo (ASTM)	12.46	4.39	0.56	0.37	0.36	0.021	0.008	0.011	0.03	–
E410NiMo (As measured)	11.6	4.5	0.529	0.44	0.38	0.023	0.01	0.01	0.014	0.003

comprehensive study on a single pass weld microstructure has already been conducted [15].

2. Materials and characterization methods

A 50 mm thick weld metal was deposited on a 50 mm thick CA6NM substrate (25 cm × 50 cm) using 13Cr4Ni flux-cored welding electrodes (E410NiMo) and a Scompi robotic welding machine [16] according to AWS A5.22 in order to reproduce the industrial condition. The welding parameters are presented in Table 1. The nominal and measured compositions of substrate and the welding electrode are shown in Table 2. The deposited weld metal was the result of 10 layers of 40 adjacent and parallel weld passes, for a total of approximately 400 passes as shown schematically in Fig. 1. Each pass was deposited in the longitudinal (X) direction beside previous pass and over the layer beneath. The welding direction was always positive X. In producing each complete layer (about 40 passes), the torch moved along the Y direction, +Y and −Y in subsequent layers. Samples used in this study have been taken from the middle of the weld.

Microstructure, chemical composition, and hardness were determined in the as-welded condition. The actual chemical composition of the weld metal and base metal were measured by a Glow Discharge Atomic Emission Spectrometer on an average surface of 4 mm^2. The elements C, N, O, and S were measured by combustion/fusion determination methods. A spectrometer operated at 15 kV with the working distance of 15 mm was used to perform chemical composition analysis of the weld layer regions, phases and inclusion particles using ESPRIT analytical software (Bruker Corporation, Germany). To reveal microstructure and austenite particles, samples were polished mechanically and then electro-polished with a solution of 65 ml $HClO_4$, 550 ml ethanol, 70 ml butyl-cellusolve, and 70 ml H_2O using an electropolishing device at 25 °C, 25 V for 20 s. The austenite volume fractions in samples were measured by X-ray diffraction from a Rietveld analysis with an X-ray diffractometer machine [17]. Hardness evaluations on large maps have been done using an automatic micro-hardness testing machine with a load of 300 g and a loading time of 10.2 s. A scanning electron microscope (SEM) operated at 5 kV to 20 kV was used to observe the samples microstructures. Electron backscattered diffraction (EBSD) technique was used to determine the grains orientations in the weld metal. The integration time was 5 ms and 2 × 2 binning was used for the acquisition and grain orientation maps were made using Tango software. Then, austenite grains reconstructions were done on EBSD maps using specific reconstruction technique [18]. Optical and SEM images were used to quantify determine dilutions and inclusions distributions in weld layers. For this, ImageJ software using threshold filtering methods was applied [19].

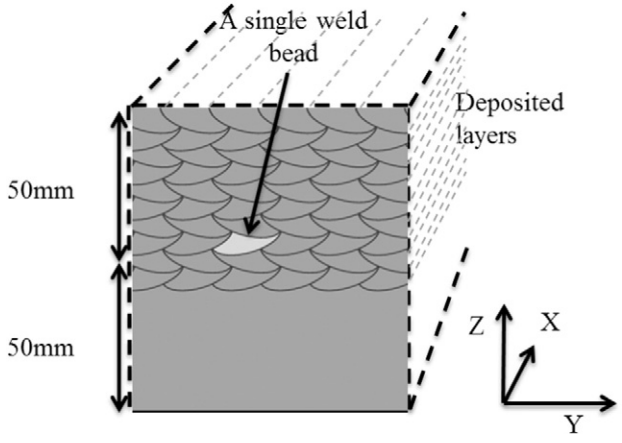

Fig. 1. Schematic cross-section of the weld layers.

3. Results and discussions

3.1. Chemical composition

The measured chemical compositions of the base metal and weld metal given in Table 2 show that there are some chemical differences between the base metal and the weld metal, however they can be

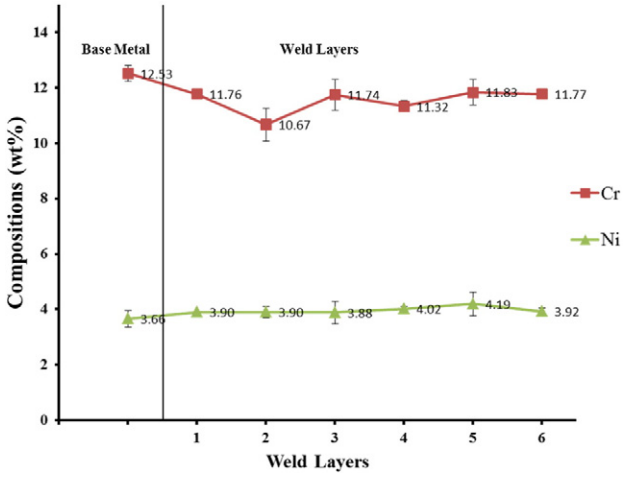

Fig. 2. Chromium and nickel contents of the base metal and the successive weld layers measured on average surfaces of 1 μm^2.

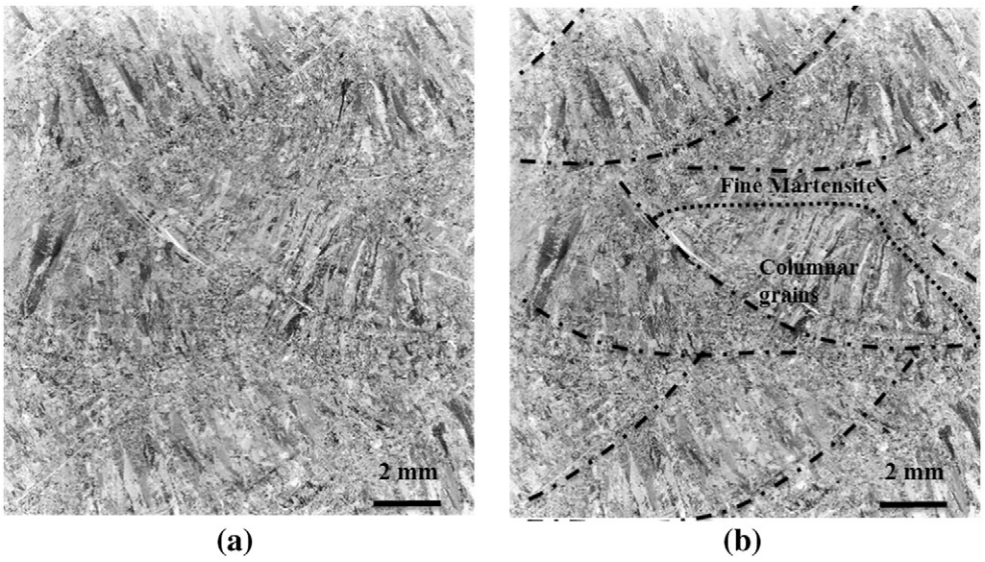

Fig. 3. (a) Microstructure of a multipass weld sample etched by Kalling's no. 2 reagent (transverse cross-section perpendicular to the weld plate which corresponds to the Z–Y plane in Fig. 1). In (b), the dashed lines represent the weld bead boundaries in (a); the dotted line separating the column-shaped and fine martensite is drawn based on microstructure observations.

both considered as 13Cr4Ni steels. The chemical composition of layers presented in Fig. 2 shows a slight composition gradient in the first weld layers. Base metal had slightly higher chromium content as compared to the weld electrode composition which dilutes gradually layer by layer moving away from the base metal. The opposite happens for the nickel content as it was slightly lower in the base metal. The chemical compositions of layers become almost the same after layer 3 and there are no obvious variations if heterogeneity and measurement errors are taken into account. The variations in chemical compositions can be explained by the heterogeneous nature of the weld metal along with the relatively small size of measured spots (about 1 μm^2).

3.2. Microstructure of the as-welded multipass sample

The microstructure of a multipass weld taken from the center of the deposited weld metal is presented in Fig. 3(a). Individual beads could be recognized in the microstructure. Regions with column-shaped packets microstructure and fine martensite microstructures can be distinguished. The fine martensite regions helps to delimitate the individual beads as presented in Fig. 3(b).

The column-shaped microstructure can be seen as features extending from the fusion line of a weld pass toward the subsequent passes. These columns are following the heat flow direction toward the surface of each bead. It is most likely that these are former austenite columnar grains traces formed from δ-ferrite solidification structure and the grains structures were not significantly modified by the martensitic transformations during cooling ($\gamma \rightarrow M$). Even in some regions in which the heat of subsequent passes has raised the temperature to austenite region, the microstructure remains as columns on cooling as it transforms back to fresh martensite again. The fresh martensite which has been formed over a formerly fresh martensite of the as-welded metal, is called double-quenched martensite and it is expected to be slightly harder than the weld fresh martensite due to higher dislocations density and additional precipitation of carbides [20]. This part of

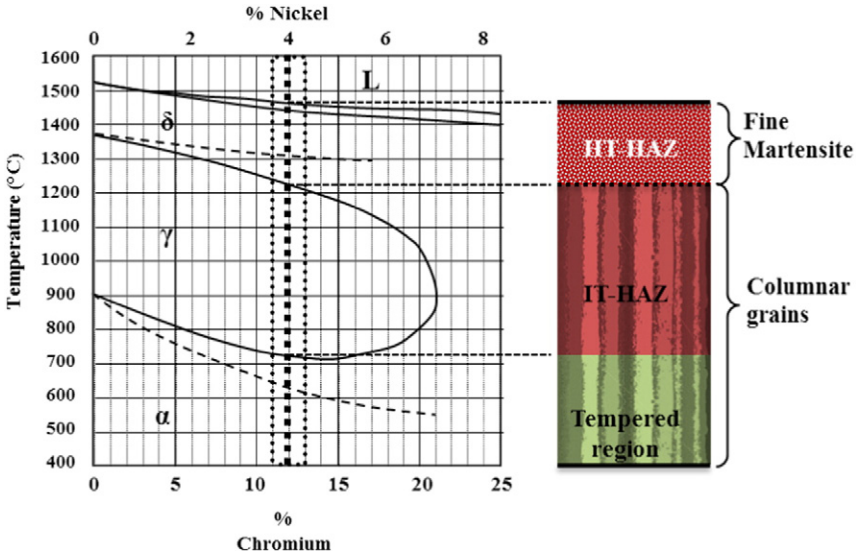

Fig. 4. Phase diagram showing the phase's domain and their corresponding HAZ inside a single weld bead (phase diagram taken from Folkhard [5]). Phase diagram dashed lines are transformation lines showing possible transformations on heating. The scheme on the right corresponds to the regions observed in a weld bead thermally affected by an adjacent single bead [15].

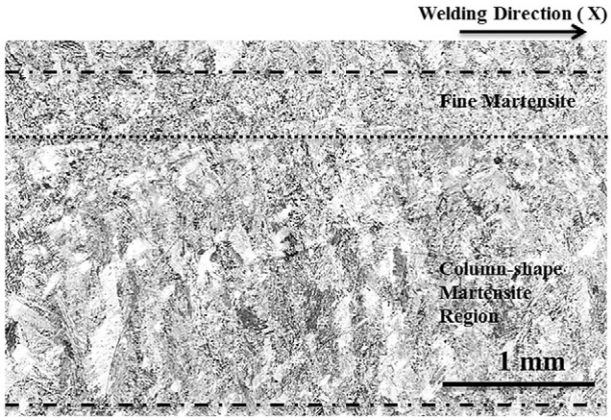

Fig. 5. Microstructure of a bead in multipass weld sample etched by Kalling's no. 2 reagent (longitudinal cross-section, perpendicular to weld plate). Dashed lines are showing the approximate weld bead boundaries. Dotted lines are separating the fine martensite and columnar region inside the weld bead.

columnar region in which double-quenched martensite can form is called intermediate temperature HAZ (IT-HAZ). Away from the fusion lines where the temperature raise is about "martensite to austenite transformation temperature on heating" (A_{C1}), the increase in temperature is just enough to produce some austenite particles and to temper the fresh martensite matrix [2]. This part of columnar region is called Tempered region. Although the tempered martensite shows lower hardness values, it is difficult to distinguish the corresponding region in an etched sample.

The fine martensite zones can be considered as areas in which the subsequent or adjacent passes was close enough to rise the temperature up to ferrite stable region. Heating above 1300 °C (approximately) has

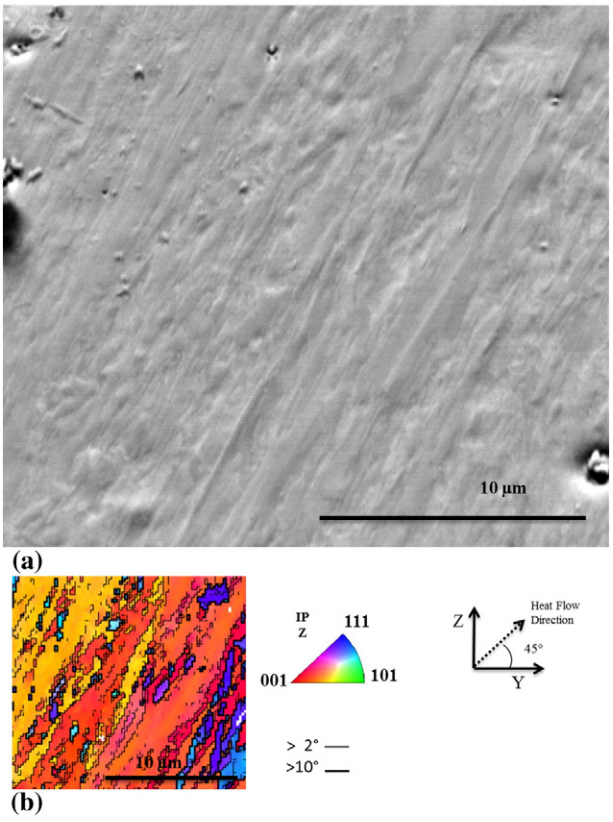

Fig. 7. (a) A typical secondary electron image (SE-SEM) in tilted conditions and at high magnification of the columnar area. (b) EBSD map of the area shown on (a).

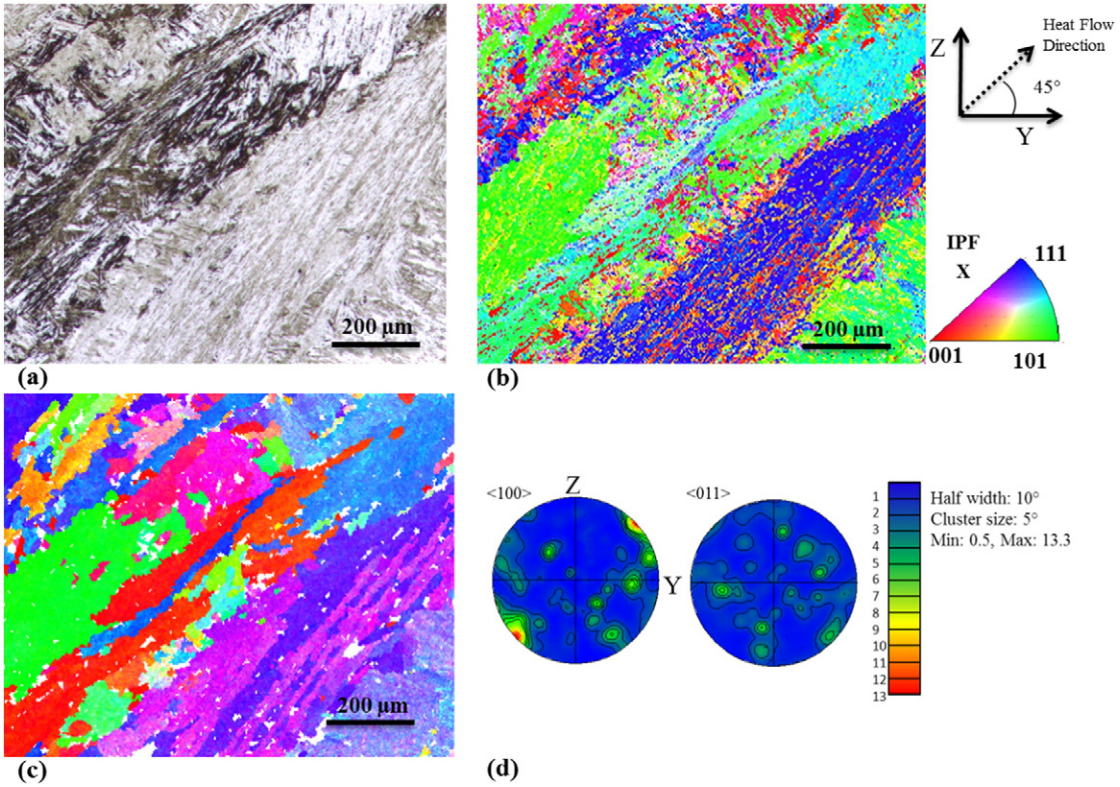

Fig. 6. Multipass weld microstructure in columnar zone. (a) Etched by Kalling's no. 2 reagent. (b) EBSD map according to the colored inverse pole figure on X direction (Fig. 1). (c) Austenite parent grain reconstruction of the EBSD map. (d) Pole figures of column-shaped martensite zone in ⟨100⟩ and ⟨011⟩ directions. The welding direction (X) is perpendicular to the images.

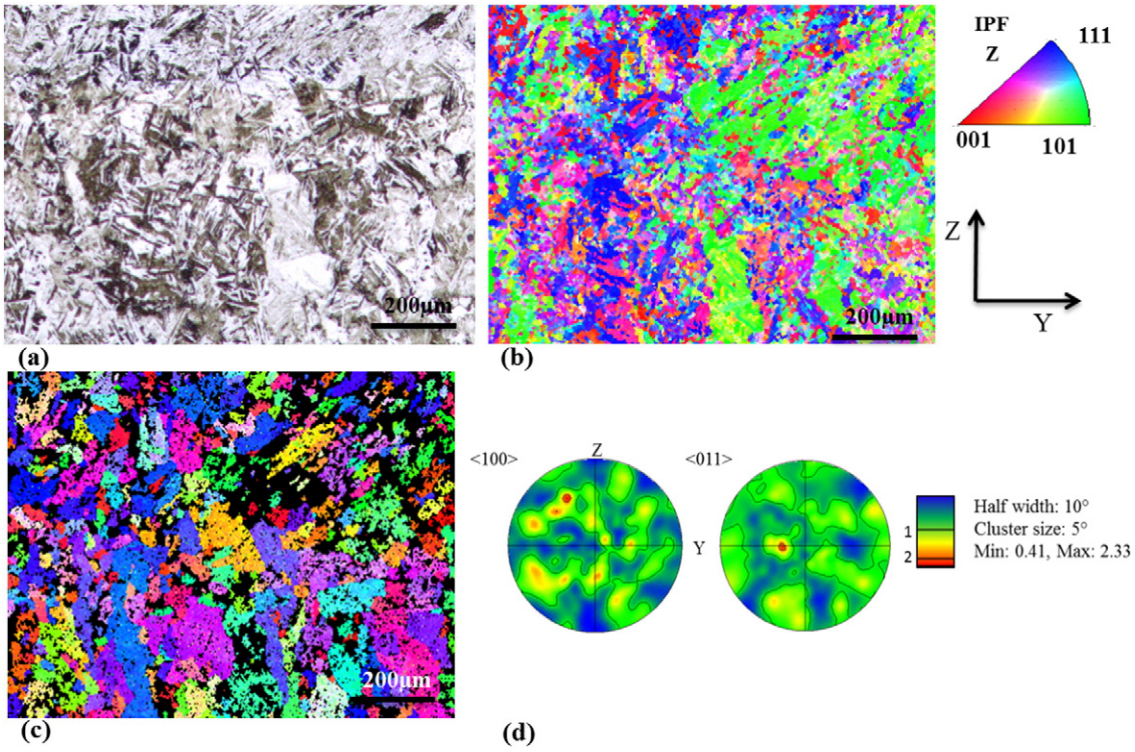

Fig. 8. Microstructure of fine martensite zone. (a) Optical microscopy image after etching by Kalling's no. 2 reagent. (b) EBSD map according to the colors invers pole figure legend of Y–Z plane (see Fig. 1) of the same region presented in (a). (c) Austenite parent grain reconstruction of the EBSD map. (d) Pole figures of fine martensite region in ⟨100⟩ and ⟨011⟩ directions. The welding direction (X) is perpendicular to the images.

changed the formerly column-shaped microstructure of packets and then it has generated smaller martensite blocks and sub-blocks after cooling to room temperature. This area was called the high temperature HAZ (HT-HAZ) [21].

Fig. 4 shows the schematic correlation of microstructure and phase diagram on heating. The simplified three-layered HAZ can be seen as HT, IT, and Tempered on this diagram corresponding to the heat effects of only one subsequent pass and the related phase transformations.

A longitudinal cross-section (Z–X plane in Fig. 1) of the multipass weld sample is presented in Fig. 5. Column-shaped packets of martensite could be seen together with a fine grain martensite zone similar to what has been shown on the transverse cross-section figure (see Fig. 3). Having column-shaped grains in both longitudinal and transversal cross-sections is the evidence for columnar dendritic solidification in weld. The fine martensite region (HT-HAZ) width is also determined to be about 500 μm for the welding conditions of current study.

3.3. EBSD analysis of multipass weld sample

The column-shaped packets and fine microstructures can be clearly revealed under EBSD. For instance, by comparing the image of etched sample with its EBSD map (Fig. 6(a) and (b)), it becomes clear that in the columnar zone, each column corresponds to a region with parallel packets and blocks of similar orientations. This confirms the assumption that a strong variant selection has been taken place in these regions during the solidification and subsequent phase transformations. Even becoming exposed to the later passes thermal cycle did not change the packets and blocks variant selection in this region.

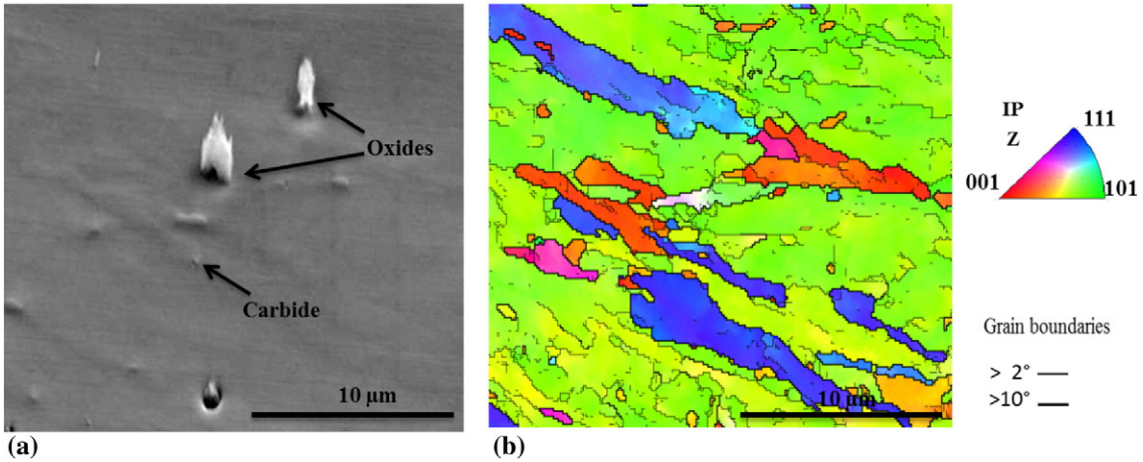

Fig. 9. (a) high magnification SEM image of fine martensite region (tilted view). (c) EBSD map of the area shown on (a).

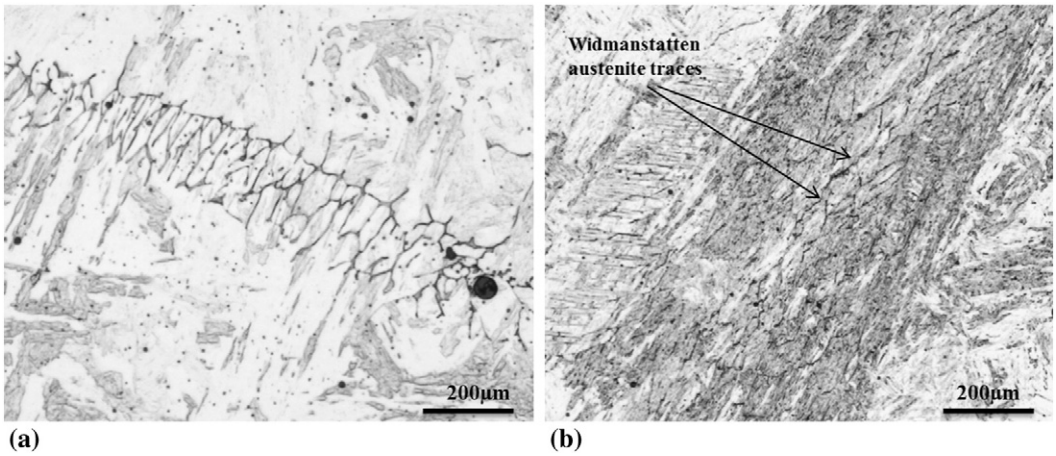

Fig. 10. (a) δ-Ferrite traces in the martensitic matrix of the multipass weld revealed by Kalling's etchant. (b) Microstructure of the multipass weld with the former Widmanstätten austenite traces that remained inside a martensite grain in the IT-HAZ regions.

The austenite grains reconstruction presented in Fig. 6(c) shows that austenite parent grains kept the expected columnar microstructure and martensite packets formed inside columnar austenite grains. The austenite grains in this region are several millimeters long in the cooling direction and about 200 µm wide. The persistence of solidification microstructure confirms that the crystallographic texture transformations from δ-ferrite to austenite and eventually to martensite were happened with strong variant selections.

Pole figures of the columnar area are presented in Fig. 6(d). Although the presence of some packets along heat flow direction created high intensities in the figures, no strong texture is observed.

A high magnification SEM and EBSD analysis can reveal the detailed microstructure of columnar area (Fig. 7). This type of microstructure can be found everywhere in the columnar region. The EBSD map shows that sub-blocks are consisted of many parallel laths of low-angle interfaces and some high-angle boundaries. The widths of the laths were measured about few hundreds of nm. These laths are revealing the complexity of the column-shaped martensite packets microstructure at high magnification.

For the fine martensite regions (HT-HAZ), the EBSD map shows a fine microstructure similar to the one revealed on the etched sample. The optical microstructure and EBSD map of the laths are presented in Fig. 8(a) and (b). The austenite parent grains reconstruction was also performed in the fine martensite zone (Fig. 8(c)). Grain reconstruction showed austenite grain modification to about 40 µm. Studies suggested that the thermal cycle of adjacent pass was high enough to trigger recovery and recrystallization stages but the grain growth reported in these studies [21] cannot be confirmed. Another hypothesis is that the transformation of austenite to delta-ferrite, and then again to austenite produced smaller austenite grains. The reason can be the fact that more nucleation sites are present compared to the initial cooling of the weld metal. Thus the former solidification microstructure disappears and a finer martensite is produced. Pole figures of this area confirm the absence of an as-welded texture (Fig. 8(d)).

SEM imaging and EBSD analysis of a fine grain microstructure at high magnification is presented in Fig. 9. Small sub-blocks were observed in SEM image with carbides precipitated at sub-block boundaries. The EBSD map shows that the sub-blocks are still consisted of parallel laths similar to columnar region. The widths of these laths also observed to be about few hundred nm. In fact in fine grain region, the heat cycle of adjacent pass breaks down the columnar microstructure into smaller sub-blocks. However, parallel interfaces are still present inside these sub-blocks.

3.4. Inhomogeneity in the weld

Heterogeneities at microscopic scale were found in the microstructure of the multipass weld; δ-ferrite traces, Widmanstätten austenite

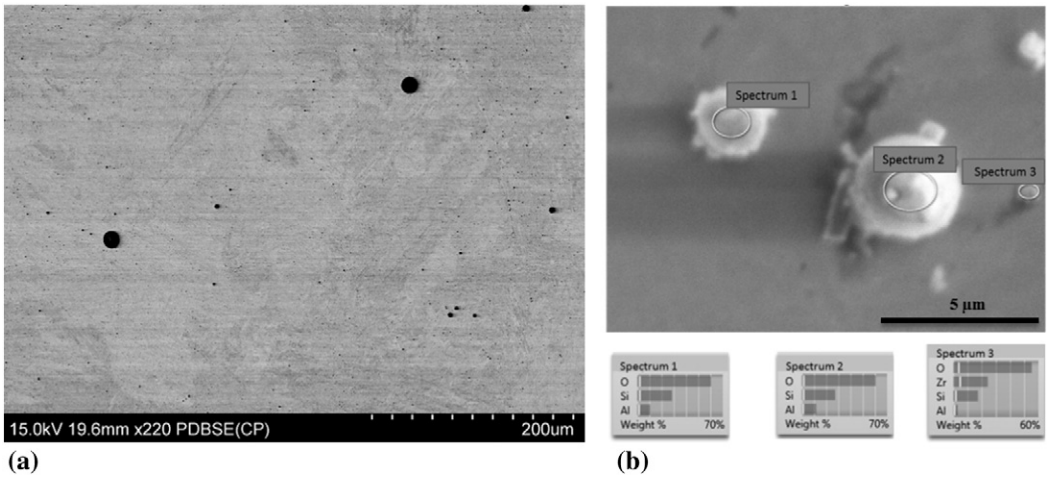

Fig. 11. (a) SEM image of etched multipass weld sample. Black circles are oxide cavities as they have been removed by mechanical polishing. (b) Example of EDX analysis of oxides found in the weld. Electropolishing method was used to preserve the oxides on the surface.

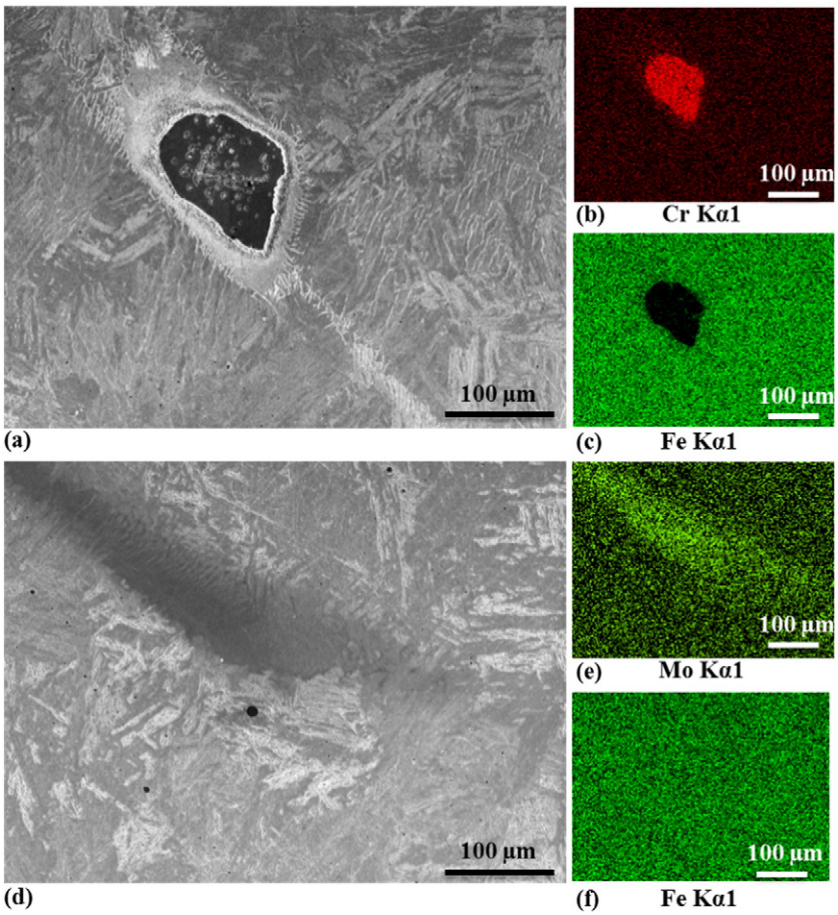

Fig. 12. (a) SEM image of a chromium particle in the weld metal. (b and c) EDX analysis of chromium and iron in area presented in (a) respectively. (d) SEM image of a molybdenum rich zone in the weld metal. (e and f) EDX analysis of molybdenum and iron in area presented in (d).

traces, oxides inclusions, carbides, and austenite particles were found in between martensitic laths. Identifying these heterogeneities helps to better understand the weld complex nature.

δ-Ferrite traces have been found in the weld as microstructures parallel to the weld lines (Fig. 10(a)). It has been shown that their formation is due to solidification segregation of semi-molten electrode enriched in high ferrite-stabilizing alloying elements [15]. They are formed during the last stage of solidification and their presence is a sign of inadequate mixing in the weld pool or an insufficient heat input.

Widmanstätten austenite traces are another type of inhomogeneity in the weld which have been found inside martensite columnar laths as shown in (Fig. 10(b)). Widmanstätten austenite has been formed during the cooling of the ferrite phase and left traces like narrow wedges starting from the boundaries of former δ-ferrite columnar grains [21]. Widmanstätten austenite then left heterogeneities in the crystal structure which was detectable after martensite transformation. Widmanstätten austenite traces in the multipass weld were found only in the IT-HAZ and no traces have been found in HT-HAZ which shows that these microstructures were erased by allowing the full transformation of the ferrite phase to take place.

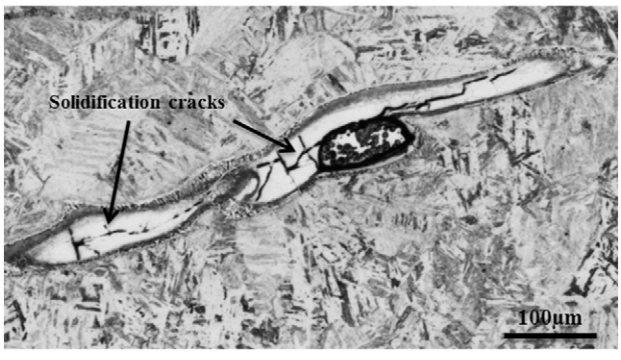

Fig. 13. Cracks in δ-ferrite phase produced by an uncompleted mixing of a chromium–nickel particle close to the weld line, revealed by Kalling's etchant.

Two types of inclusions have been found in the weld metal of current study: oxide inclusions which are round particles evenly distributed and un-molten alloying compounds coming from the electrode.

The oxide inclusions are circular inclusions which were found all over the weld metal (Fig. 11(a)). Composition analysis showed that these particles consisted of aluminum, silicon, and zirconium oxides (Fig. 11(b)). These oxides were formed by oxidizing chemical reactions in the weld pool. The image analysis showed that oxide inclusions have about a 0.01% volume fraction and 97% of their population have less than one micrometer in diameter. The oxide inclusions are helpful determining the weld fusion lines.

The second type of inclusions found in the weld was compounds enriched in chromium, nickel, or molybdenum. These particles were found in areas close to the boundaries between adjacent weld passes. They are semi-melted particles coming from the filler materials. As the elements found in these particles are ferrite stabilizing elements, they promote the formation of δ-ferrite phase and dendritic ferrite microstructures around them during cooling. Fig. 12(a, b, and c) shows a chromium particle in the weld metal. Although the particle was not melted, it produced δ-ferrite phase around it and traces of δ-ferrite solidification dendrites can be seen. Fig. 12(d, e, and f) shows an incomplete melting

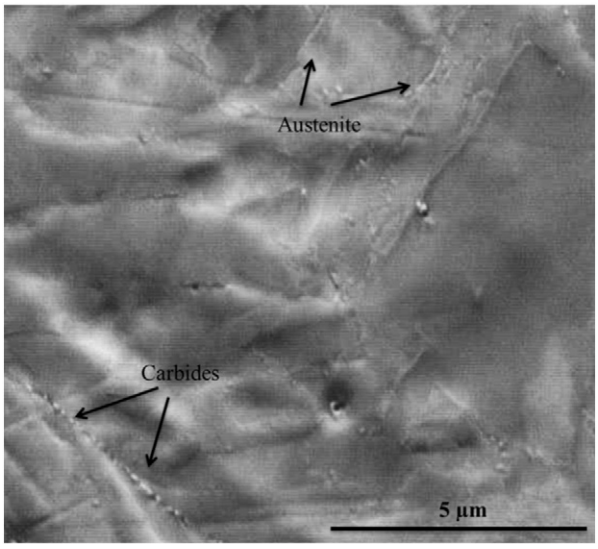

Fig. 14. SEM (SE) image of multipass weld showing carbide and austenite particles.

of a ferromolybdenum particle which also formed solidification dendrites. No δ-ferrite phase was stable in this case.

Cracks have also been found in δ-ferrite phases around chromium-nickel particles. The lower solidification temperature of stable δ-ferrite phase and its lower yield strength make it susceptible to cracking [14,22]. Fig. 13 shows an example of this type of cracks. These cracks may have been produced during austenite to martensite transformation as it has been reported recently [23]. Then the formation of stable δ-ferrite during solidification of the weld metal is a major concern and can deteriorate ductility, toughness, and fatigue properties of the steel as it leaves a pre-crack in the welded joint [23].

Nanometer-size carbides were also found in the as-welded multipass samples (Fig. 14). As it has been reported that there is no sign of carbides in a 13Cr4Ni single pass [15], their presence in a multipass weld suggests that thermal cycle of subsequent weld passes enhances their formation. Carbide particles were found mostly in HT-HAZ sub-block interfaces (see also Fig. 9).

Austenite particles have also been found in the weld metal in IT-HAZ areas of multipass sample (Fig. 14) and identified by EBSD analysis. These austenite particles were revealed using electropolishing techniques and they are always associated with the presence of chromium carbides in the neighborhoods. As there was no trace of austenite in an as-welded single pass sample [15], these austenite particles were formed from martensite reversed transformation to austenite and they are called reformed austenite. It has been reported that the reformed austenite remains stable at room temperature due to local enrichment of chromium and nickel atoms and that their presence in the multipass weld is a favorable feature [2,12,24,25].

3.5. Hardness

In order to characterize the local properties of the weld and relate them to the microstructure variations identified in the previous section, hardness maps have been made on the multipass pass sample (Fig. 15(a)). These maps present different hardness distribution layout inside beads compared to the results reported previously by the authors in a single and double weld pass beads [15]. A repetitive red pattern can be recognized surrounded by green bands. It is most likely that the green bands represent areas in which the collective heat of subsequent passes had a tempering effect and the red regions are the areas in which the subsequent passes produced fresh martensite. This hypothesis could be tested by studying the microstructures of each region.

Neither a green band nor a single red region belongs to a single bead. In fact, Fig. 15(a) shows that by considering the approximative locations of the fusion lines, more regions can be distinguished on a single bead. These regions could be explained by considering the accumulative heat effects of the exact subsequent weld pass and the 3 passes of the above layer.

The correlation between microstructure and hardness is schematically presented in Fig. 15(b). Six regions can be recognized in each weld pass by projecting the microstructure (described in Fig. 3) on the regions identified in the hardness map. These six regions are discussed in details as follows.

In region (a), the original columnar grains of the pass were replaced by a fine and fresh martensite due to the first subsequent pass. Later it receives some tempering heat from the second and the third passes, enough to temper the fresh martensite. Thus region (a) has a fine and tempered microstructure with hardness values of a tempered martensite.

In region (b) as in region (a), a fine and fresh martensite microstructure was produced by the first pass. This region is located in the HT-HAZ of the second and third passes but it is far from the 4th pass, then it stays a fine and fresh martensite. It has hardness values slightly higher than that of typical fresh martensite as a double-austenitization has taken place leading to a finer fresh martensite.

In region (c), the original columnar microstructure is transformed to a fine martensite microstructure by the third pass, but later it becomes tempered by the 4th pass. A fine and tempered microstructure and hardness values similar to region (a) are expected here.

In region (d), a fine and fresh martensite microstructure was produced by the third and the 4th passes. Hardness values of a fine and fresh martensite are expected similar to region (b).

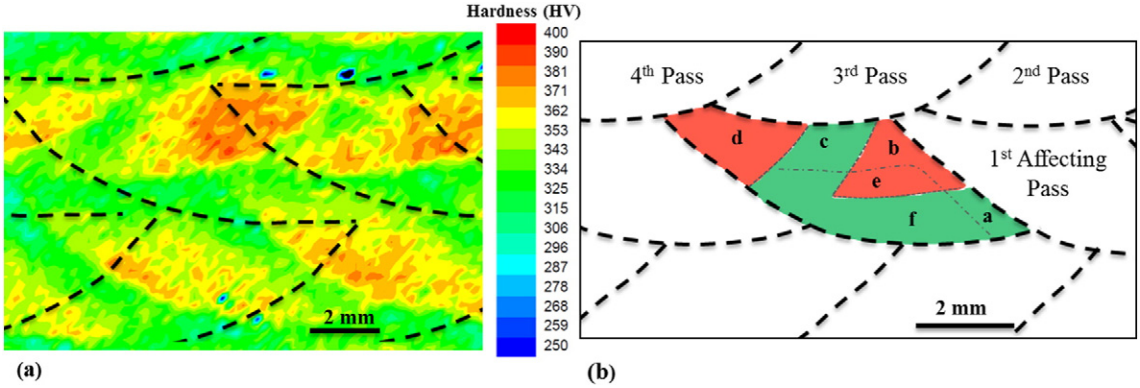

Fig. 15. (a) 2D Hardness maps of the multipass sample (30 points/mm^2) with dashed lines showing the approximative locations of weld lines. (b) Schematic presentation of regions in a single weld bead based on both microstructure and hardness.

The region (e) is located in the IT-HAZ of the second and the third passes having a double-quenching effect on microstructure of this region. Hardness values of double-quenched martensite is expected here which is as high as fresh martensite.

In region (f), the original columnar microstructure of the bead was located far from all of the surrounding passes and it received only tempering heats which led to the lowest hardness of all regions. This is the region in which the reformed austenite formation was observed.

The current study showed that a multipass weld microstructure has a complex microstructure consisting of various regions with different heat treatment histories altogether with micro-scale heterogeneities. Although the simplified HAZ consisting of three thermal cycle region (HT, IT and Tempered HAZ) can explain the overall microstructure and the hardness map, the actual microstructure is certainly more complicated if the precise HAZ locations are considered. These results confirm that any mechanical evaluation in the weld region should be done with great cautions.

4. Conclusions

This study showed that a multipass weld microstructure is much more complicated than a single pass weld. The microstructure of the 13Cr4Ni multipass weld consists of two main regions, one having a fine martensite microstructure and the other a column-shaped martensite packets. In the middle of the multilayer weld, each of these two regions can be divided in several regions affected in different ways by subsequent weld passes. It has been shown that with the current study's weld passes configuration, the heat effects of immediate next pass and the three passes of the above layer can be used to explain the weld bead microstructure. The changes in hardness can be explained by variations in microstructure and local texture, based on the amount of heat received in different regions. Austenite parent grain partial recrystallization and carbides formation were observed. Solidification cracks inside delta ferrite particles were reported which showed the importance of implementing proper welding parameters. The various regions of the multipass weld were detailed from the hardness map with the aid of a simplified three-layered heat affected zone configuration, consisting of a high, an intermediate, and a tempered zone. This study presented the multipass weld heterogeneous and complex microstructure which proves that any overall mechanical evaluation should be done with great cares.

Acknowledgments

The authors would like to acknowledge Natural Sciences and Engineering Research Council of Canada (NSERC), Institut de Recherche d'Hydro-Québec (IREQ), Alstom Power Co., and École de Technologie Supérieure (ÉTS) (RDCPJ 386936 - 09) for the technical and financial supports.

References

[1] J.C. Lippold, D.J. Kotecki, Welding Metallurgy and Weldability of Stainless Steels, John Wiley & Sons, 2005.
[2] D. Thibault, P. Bocher, M. Thomas, Residual stress and microstructure in welds of 13%Cr–4%Ni martensitic stainless steel, J. Mater. Process. Technol. 209 (4) (2009) 2195–2202.
[3] D. Thibault, et al., Residual stress characterization in low transformation temperature 13%Cr–4%Ni stainless steel weld by neutron diffraction and the contour method, Mater. Sci. Eng. A 527 (23) (2010) 6205–6210.
[4] H. Zheng, et al., Effect of carbon content on microstructure and mechanical properties of hot-rolled low carbon 12Cr–Ni stainless steel, Mater. Sci. Eng. A 527 (27–28) (2010) 7407–7412.
[5] E. Folkhard, Welding Metallurgy of Stainless Steels, Springer-Verlag, Berlin, 1988.
[6] W. Wu, et al., Relationship between alloying elements and retained austenite in martensitic stainless steel welds, Scr. Mater. 42 (2000) 1071–1076 (Compendex).
[7] G.F.V. Voort, Martensite and retained austenite, Ind. Heat. 76 (2009) 51–54 (The Institution of Engineering and Technology).
[8] M.C. Tsai, et al., Phase transformation in AISI 410 stainless steel, Mater. Sci. Eng. A A332 (1–2)) (2002) 1–10.
[9] D. Thibault, et al., Reformed austenite transformation during fatigue crack propagation of 13%Cr–4%Ni stainless steel, Mater. Sci. Eng. A 528 (21) (2010) 6519–6526.
[10] D.-N. Zou, et al., Influence of tempering process on mechanical properties of 00Cr13Ni4Mo supermartensitic stainless steel, J. Iron Steel Res. Int. 17 (8) (2010) 50–54.
[11] D. Thibault, et al., Reformed austenite transformation during fatigue crack propagation of 13%Cr–4%Ni stainless steel, Mater. Sci. Eng. A 528 (21) (2011) 6519–6526.
[12] P.D. Bilmes, C. Llorente, M. Solari, Effect of Post Weld Heat Treatments on the Microstructure and Mechanical Behaviour of 13Cr–4NiMoL and 13Cr–6NiMoL Weld Metals, ASM International, Cincinatti, OH, United States, 1998.
[13] Y.Y. Song, et al., Microstructural evolution and low temperature impact toughness of a Fe–13%Cr–4%Ni–Mo martensitic stainless steel, Mater. Sci. Eng. A 527 (3) (2010) 614–618.
[14] P.D. Bilmes, M. Solari, C.L. Llorente, Characteristics and effects of austenite resulting from tempering of 13Cr–NiMo martensitic steel weld metals, Mater. Charact. 46 (4) (2001) 285–296.
[15] M. Mokhtabad Amrei, et al., Microstructure characterization of single and multipass 13Cr4Ni steel welded joints, Metallography, Microstructure, and Analysis (2015) 1–12.
[16] Hydro-Québec, I.d.r., Scompi Robot, Robotic system for generating station work, U. Patent, Editor. 2011: Canada.
[17] H.M. Rietveld, A profile refinement method for nuclear and magnetic structures, J. Appl. Crystallogr. 2 (2) (1969) 65–71.
[18] L. Germain, et al., An advanced approach to reconstructing parent orientation maps in the case of approximate orientation relations: application to steels, Acta Mater. 60 (11) (2012) 4551–4562.
[19] W.S. Rasband, ImageJ, U.S. National Institutes of Health, 1997–2012.
[20] G.E. Totten, Steel Heat Treatment Metallurgy and Technologies, second ed. Taylor and Francis, Portland, 2007 832.
[21] D. Carrouge, Phase Transformations in Welded Supermartensitic Stainless Steels, University of Cambridge, 2002.
[22] P. Wang, et al., Effect of delta ferrite on impact properties of low carbon 13Cr–4Ni martensitic stainless steel, Mater. Sci. Eng. A 527 (13–14) (2010) 3210–3216.
[23] M. Paquin, et al., Assessment of cold cracking tests for low transformation temperature martensitic stainless steel multipass welds, Welding in the World (2015) 1–12.
[24] Y. Song, et al., Formation of the reversed austenite during intercritical tempering in a Fe–13%Cr–4%Ni–Mo martensitic stainless steel, Mater. Lett. 64 (13) (2010) 1411–1414.
[25] Y. Song, et al., The influence of tempering temperature on the reversed austenite formation and tensile properties in Fe–13%Cr–4%Ni–Mo low carbon martensite stainless steels, Mater. Sci. Eng. A 528 (12) (2011) 4075–4079.